International Journal of Heat and Mass Transfer 140 (2019) 331–345

Contents lists available at ScienceDirect

International Journal of Heat and Mass Transfer

journal homepage: www.elsevier.com/locate/ijhmt

Fluid-structure interaction analysis of entropy generation and mixed convection inside a cavity with flexible right wall and heated rotating cylinder

A.I. Alsabery [a,b,*], F. Selimefendigil [c], I. Hashim [b], A.J. Chamkha [d], M. Ghalambaz [e,f]

[a] Refrigeration & Air-conditioning Technical Engineering Department, College of Technical Engineering, The Islamic University, Najaf, Iraq
[b] Centre for Modelling & Data Science, Faculty of Science & Technology, Universiti Kebangsaan Malaysia, 43600 UKM Bangi, Selangor, Malaysia
[c] Department of Mechanical Engineering, Celal Bayar University, 45140 Manisa, Turkey
[d] Mechanical Engineering Department, Prince Sultan Endowment for Energy & Environment, Prince Mohammad Bin Fahd University, Al-Khobar 31952, Saudi Arabia
[e] Department for Management of Science and Technology Development, Ton Duc Thang University, Ho Chi Minh City, Vietnam
[f] Faculty of Applied Sciences, Ton Duc Thang University, Ho Chi Minh City, Vietnam

ARTICLE INFO

Article history:
Received 24 February 2019
Received in revised form 28 April 2019
Accepted 1 June 2019
Available online 10 June 2019

Keywords:
Unsteady mixed convection
Entropy generation
Rotating cylinder
Elastic wall
Finite element method

ABSTRACT

The current work concentrates on the transient entropy generation and mixed convection due to a rotating hot inner cylinder within a square cavity having a flexible side wall by using the finite element method and arbitrary Lagrangian-Eulerian formulation. Effects of various relevant parameters like Rayleigh number ($10^4 \leqslant Ra \leqslant 10^7$), angular rotational velocity ($-1 \leqslant \Omega \leqslant 1$), dimensionless elasticity modulus ($10^{12} \leqslant E \leqslant 10^{15}$) on the convective heat transfer characteristics and entropy generation rates are analyzed for dimensionless time $10^{-8} \leqslant \tau \leqslant 3.5$. It is observed that various complex shaped wall deformations are established depending on the non-dimensional elastic modulus of the flexible right wall and cylinder rotation direction. The local and average Nusselt numbers rise with *Ra* and secondary peaks in the local Nusselt number are established for lower values of *Ra*. The local heat transfer along the hot cylinder does not change for the case of clockwise rotation of the heated cylinder even if there is a wall deformation in the positive *x*-direction. The highest average heat transfer and global entropy generation rates are achieved for the case of counter-clockwise rotation of the circular cylinder and for lower values of the flexible wall deformation.

1. Introduction

Mixed (combined) convection flow and heat transfer within various cavities are an important area of research for the improvement of the energy efficiency and the reduction of the energy consumption in a lot of engineering systems and equipments. Such applications are solar collectors, lubrication technologies, heat exchangers, ventilation, building insulation and drying technologies. In comparison with other modes of convection, mixed convection is considered to be more complicated because of the combination of the buoyancy force which is caused by the difference in temperature and the shear force that is resulting from the movement of the wall(s) [1]. Öztop and Dagtekin [2] reported the mixed convection heat transfer in a double lid-driven vertically-heated square cavity under steady-state conditions. They observed that the rate of the heat transfer was enhanced as a result of moving the vertical walls of the considered cavity in reverse directions. On the other hand, the same direction movement of the vertical walls produced a reduction in the heat transfer. Talebi et al. [3] considered mixed convection flow and heat transfer in a top lid-driven square cavity filled with a nanofluid. Abu-Nada and Chamkha [4] considered mixed convection water-Al_2O_3 nanofluid in an inclined lid-driven square cavity. The problem of mixed convection of a micropolar fluid over a stretched surface was studied by Rashad et al. [5], whose work was later extended to the inclined case by Ramesh et al. [6]. In a recent study, Raju et al. [7] have considered the problem of mixed convection over a stretched surface under transient conditions. Chamkha et al. [8] and Alsabery et al. [1] carried out numerical investigations for mixed convection inside a lid-driven cavity that

* Corresponding author at: Centre for Modelling & Data Science, Faculty of Science & Technology, Universiti Kebangsaan Malaysia, 43600 UKM Bangi, Selangor, Malaysia.
E-mail addresses: ammar_e_2011@yahoo.com (A.I. Alsabery), mohammad.ghalambaz@tdtu.edu.vn (M. Ghalambaz).

https://doi.org/10.1016/j.ijheatmasstransfer.2019.06.003
0017-9310/

Nomenclature

Cp	specific heat capacity
$\mathbf{d}_s$	displacement vector
E	dimensionless elasticity modulus
E_τ	dimensional Young's modulus
$\mathbf{F}_v$	body force vector
$\mathbf{g} = (0, -g)$	acceleration of the gravity
GEG	dimensionless global entropy generation
h	coefficient of the heat transfer
k	thermal conductivity
K_r	thermal conductivity ratio
L	width and height of cavity
$\overline{Nu}$	average Nusselt number
Pr	Prandtl number
r & R	radius of the heated rotating cylinder dimensionless radius of the heated rotating cylinder
Ra	Rayleigh number
S_{gen}	entropy generation rate
S_{GEN}	dimensionless entropy generation rate
S_θ	dimensionless entropy generation due to the heat transfer irreversibility
S_Ψ	dimensionless entropy generation due to the nanofluid friction irreversibility
t	dimensional time
t_P	dimensionless thickness of the flexible wall
t_p^*	dimensional thickness of the flexible wall
T	temperature
$\mathbf{u}$	velocity vector
u, v	dimensionless components of $\mathbf{u}$ in the X-direction and Y-direction
x, y & X, Y	space coordinates & dimensionless space coordinates
$\mathbf{w}$	moving coordinate velocity

Greek symbols

α	thermal diffusivity
β	thermal expansion coefficient
ε	strain
θ	dimensionless temperature
λ	Lame's first constant
μ	dynamic viscosity
ν	kinematic viscosity
ρ	density
τ	dimensionless time
ψ & Ψ	stream function & dimensionless stream function
ω & Ω	angular rotational velocity, dimensionless angular rotational velocity

Subscript

c	cold
f	fluid
h	hot
s	solid

Superscripts

$*$	dimensional parameters

filled with nanofluid. Both horizontal walls of the cavity were moving with a steady velocity. Kareem and Gao [9] reported on three-dimensional flow in a lid-driven cavity. Alsabery et al. [10] reported the problem of unsteady mixed convection in a double lid-driven wavy cavity having a nonhomogeneous nanofluid model and solid circular cylinder.

In all of the above mentioned investigations, the wall was assumed smooth and symmetric. Thus, a non-zero velocity boundary condition can be used to describe the wall's motion. This makes a moving grid unnecessary. Since the shape of the wall is not influenced by the interaction between the wall and the fluid, the problem is called one-way problem. However, there are many situations in which the fluid and the geometric structure have a mutual effect on each other, such as in the shape of the structure and the fluid flow characteristics. This area of study is known as Fluid-Structure Interaction (FSI) which takes into account the continuous deformation due to the changes in the shape of the moveable or deformable surface. In these situations, a moving grid is used to track the changes in the fluid space. In this case, the grid points are relocated to match the moving or deforming surfaces using the Lagrangian transport method. In recent years, FSI approach has been the interest of many studies due to its wide applications in mechanical, aerospace and biomedical engineering problems [11]. Such applications are flow through elastic pipes, flow through diaphragm pump, moving pistons of fluids in elastic containers, diaphragm sensors and flow through blood vessels [12,13]. Shi and Khodadadi [14,15] studied the effect of an oscillating thin fin on the flow and heat transfer in a lid-driven square enclosure. Gomes and Lienhart [16] investigated the problem of FSI in laminar and turbulent flows induced by the oscillation of flexible structures. A new type of flexible heat sink was patented by Ku [17]. Whereas the magnetohydrodynamic (MHD) effect and two-phase nanofluid model on convective heat transfer in a discretely heated square cavity with conductive inner block was reported by Alsabery et al. [18].

Soti et al. [19] showed an enhancement in heat transfer by a large-scale flow-induced deformation of a thin flexible structure. Ghalambaz et al. [20] investigated the influence of an oscillating highly thermally conductive flexible fin on the heat transfer in an enclosure. They showed in particular that a horizontal fin did not produce a significant heat transfer enhancement. Dey et al. [21] made an experimental observation on the study of the viscoelastic fluid-structure interactions. They found that the flexible structure of the viscoelastic fluids became unstable in the absence of fluid inertia. Selimefendigil and Öztop [22] and Selimefendigil et al. [23] gave further confirmation that the interaction between a fluid and a flexible surface influenced both the flow patterns as well as the shape of the surface. Raisi and Arvin [24] investigated the effect of a flexible horizontal baffle in an enclosure. In this investigation, the flexible part was embedded in the domain. Due to the interaction with the fluid, the baffle in the enclosure was subjected to small deformations. The obtained results showed that the baffle's flexibility and its size greatly influenced the convection heat transfer in the enclosure. Raisi and Arvin [24] considered the effects of a thin baffle and a top elastic wall on transient natural convection of air in a cavity. The thermal performance of the cavity depended on the baffle's length and flexibility, and the Rayleigh number. Ismael and Jasim [25] studied mixed convection in a cavity having an inlet and an outlet, with a flexible fin attached to the bottom wall. They found that the flexible fin case yielded more enhancements in the heat transfer rate than that of the rigid fin. On the other hand, for the purpose of energy saving, it is important to employ the maximum available energy from thermal systems. Entropy generation regarding to the thermodynamic constraints is used to evaluate such a performance [26]. Several reasons beyond entropy generation in applied thermal engineering that clearly described in [27–30].

Convective heat transfer of rotating systems are important in many situations such as mixing devices, turbo machinery, and drilling of oil wells [31]. Fu et al. [32] presented a numerical study on the effect of a rotating circular cylinder on the enhancement of the convective heat transfer inside a 2D cavity. Ghaddar [33] considered a rotating cylindrical heat source embedded within the center of a rectangular cavity. They found that the location of the cylinder could affect the heat transfer. An experiment of mixed convection in a rectangular cavity with a rotating plate inserted in the middle was done by Kimura et al. [34]. The situation of mixed convection in a lid-driven square enclosure having an inner circular body was investigated by Oztop et al. [35] who found that the inner circular body can control heat and fluid flow. A two-dimensional numerical study on forced convection heat transfer across a uniformly heated rotating circular cylinder have been investigated by Paramane and Sharma [36]. It was concluded that rotation of the circular cylinder can be used as a heat transfer suppression technique. Costa and Raimundo [37] concluded that the presence of a rotating cylinder in an enclosure had a significant effect on the thermal performance of the enclosure. In addition, the thermophysical properties of the rotating cylinder could control the heat transfer process. Furthermore, Hussain and Hussein [38] reported that the position of the rotating cylinder inserted in a cavity can control the heat transfer inside the considered cavity. The purpose of the cylinder rotation was identified to reduce the heat transfer rate as explained numerically by Liao and Lin [39]. Chatterjee et al. [40] performed simulation of mixed convection in a lid-driven cavity containing a thermally insulated rotating circular cylinder within the center and filled with a nanofluid. The authors showed that the cylinders rotational speed is the main factor affecting the heat transfer. Recently, Khanafer and Aithal [41] showed that the angular velocity of the inner rotating cylinder in a lid-driven cavity increased the average Nusselt number. Alsabery et al. [31] investigated the entropy generation in a porous cavity with a heated bottom wavy wall and having an inclusive rotating solid cylinder.

To the authors' best knowledge, entropy generation and mixed convection in a cavity having a flexible wall and rotating inner circular cylinder has never been reported before. Thus, the aim of the current work is to study the FSI on entropy generation and mixed convection in a cavity having a flexible right wall and heated inner rotating circular cylinder.

2. Mathematical formulation

The 2D transient laminar flow of mixed convection for viscous incompressible Newtonian fluid contained in a square cavity with side L is described in Fig. 1. A heated rotating circular cylinder with radius r and temperature T_h is inserted in the center of the cavity. The left wall is rigid and the right wall is assumed flexible. Both the vertical walls are maintained at a fixed cold temperature T_c. The horizontal walls are insulated. The fluid's thermophysical properties are constant, except for the density which obeys the Boussinesq approximation.

Using the Arbitrary Lagrangian-Eulerian (ALE) formulation, the dimensional governing equations can be written as [42]:

$$\nabla^* \cdot \mathbf{u}^* = 0, \tag{1}$$

$$\frac{\partial \mathbf{u}^*}{\partial t} + (\mathbf{u}^* - \mathbf{w}^*) \cdot \nabla^* \mathbf{u}^* = -\frac{1}{\rho_f} \nabla^* P^* + \nu_f \nabla^{*2} \mathbf{u}^* + \beta \mathbf{g}(T - T_c), \tag{2}$$

$$\frac{\partial T}{\partial t} + (\mathbf{u}^* - \mathbf{w}^*) \cdot \nabla^* T = \alpha_f \nabla^{*2} T. \tag{3}$$

Here $\mathbf{u}^*$ denotes the fluid velocity vector, $\mathbf{w}^* = (u_s^*, v_s^*)$ is the moving coordinate system velocity vector, P^* is the fluid pressure, T is the fluid/solid temperature, ρ_f is the fluid density, ν_f is the kinematic viscosity, α_f is the fluid's thermal diffusivity, α_s is the solid's thermal diffusivity, $\mathbf{g}$ is the gravitational acceleration, and β is the volumetric thermal expansion coefficient.

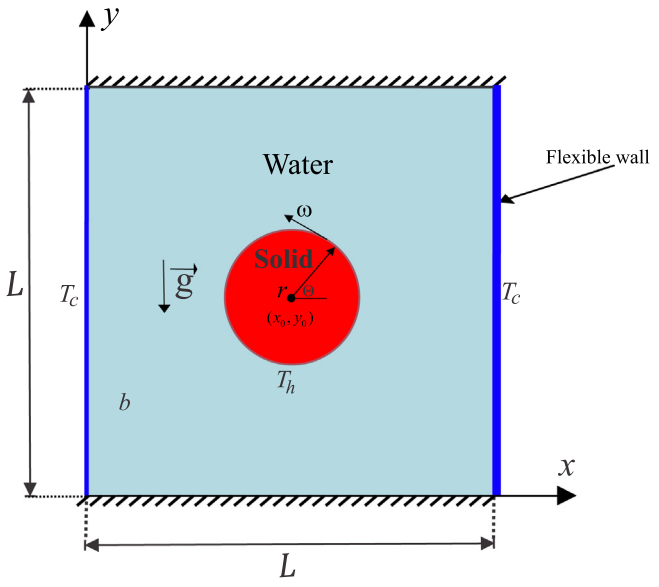

Fig. 1. Physical model of convection in a cavity with a flexible right wall and coordinate system.

The flexible wall's structural displacement is described by [13]:

$$\rho_s \frac{d^2 \mathbf{d}_s^*}{dt^2} - \nabla^* \sigma^* = \mathbf{F}_v^*, \tag{4}$$

where $\mathbf{d}_s^*$ denotes the solid displacement vector, σ^* represents the stress tensor and $\mathbf{F}_v^*$ is the applied body force. The flexible wall is assumed hyper-elastic. The stress tensor in Eq. (4) is defined using the Neo-Hookean solid model:

$$\sigma^* = J^{-1} F S F^T. \tag{5}$$

Here

$$F = \left(I + \nabla^* \mathbf{d}_s^*\right), J = \det(F) \text{ and } S = \frac{\partial W_s}{\partial \varepsilon}, \tag{6}$$

where T denotes matrix transpose. The strain energy density function W_s and the strain ε are respectively given by:

$$W_s = \frac{1}{2}\mu_l (J - I_l - 3) - \mu_l \ln(J) + \frac{1}{2}\lambda (\ln(J))^2, \tag{7}$$

$$\varepsilon = \frac{1}{2}\left(\nabla^* \mathbf{d}_s^* + \nabla^* \mathbf{d}_s^{*T} + \nabla^* \mathbf{d}_s^{*T} \nabla^* \mathbf{d}_s^*\right), \tag{8}$$

where $\mu_l = E_\tau/(2(1+\nu))$ is the Lame second constant and $\lambda = E_\nu/[(1+\nu)(1-2\nu)]$ is the Lame first constant, E the Young modulus, ν Poisson's ratio, and I_l the initial invariant of the right Cauchy-Green deformation tensor. At the flexible wall, we have the continuity of kinematic forces and dynamic motions:

$$\frac{\partial \mathbf{d}_s^*}{\partial t} = \mathbf{u}^*, \quad \sigma^* \cdot \mathbf{n} = -P^* + \mu_f \nabla^* \mathbf{u}^*. \tag{9}$$

Assuming there is no energy generation and storage at the flexible wall, the energy equation for the flexible wall can be written as:

$$\frac{\partial T}{\partial \mathbf{n}} \text{ and } T = T_c, \tag{10}$$

where $\mathbf{n}$ denotes the unit vector perpendicular to the right flexible wall.

Upon introducing the dimensionless variables:

$$X=\frac{x}{L},\ Y=\frac{y}{L},\ \mathbf{u}=\frac{\mathbf{u}^*L}{\alpha_f},\ \mathbf{w}=\frac{\mathbf{w}^*L}{\alpha_f},\ \nabla=\frac{\nabla^*}{L},\ \nabla^2=\frac{\nabla^{*2}}{L^2},$$
$$\theta=\frac{T-T_c}{T_h-T_c},\ \mathbf{d}_s=\frac{\mathbf{d}_s^*}{L},\ \sigma=\frac{\sigma^*}{E^*},\ t_p=\frac{t_p^*}{L^2},\ \tau=\frac{t\alpha_f}{L^2},\ P=\frac{L^2}{\rho_f\alpha_f^2}P^*,\quad (11)$$
$$\mathbf{F}_v^*=\frac{(\rho_f-\rho_s)Ig}{E_v},\ E=\frac{E_vL^2}{\rho_f\alpha_f^2},\ Ra=\frac{g\rho_f\beta(T_h-T_c)L^3}{\mu_f\alpha_f},\ \rho_r=\frac{\rho_f}{\rho_s}.$$

We obtain the dimensionless governing equations:

$$\frac{1}{\rho_r}\frac{d^2\mathbf{d}_s}{d\tau^2}-E\nabla\sigma=E\mathbf{F}_v, \quad (12)$$
$$\nabla\cdot\mathbf{u}=0, \quad (13)$$
$$\frac{\partial\mathbf{u}}{\partial\tau}+(\mathbf{u}-\mathbf{w})\cdot\nabla\mathbf{u}=-\nabla P+Pr\nabla^2\mathbf{u}+PrRa\theta, \quad (14)$$
$$\frac{\partial\theta}{\partial\tau}+(\mathbf{u}-\mathbf{w})\cdot\nabla\theta=\nabla^2\theta, \quad (15)$$

where $Pr=\nu_f/\alpha_f$ is the Prandtl number, $\rho_r=\rho_f/\rho_s$ the thermal diffusivity ratio and $\alpha_r=\alpha_f/\alpha_s$ the density ratio parameters. In the current work, the influence of the buoyancy force on the flexible right wall is neglected (i.e. $\mathbf{F}_v=0$).

The dimensionless boundary conditions of Eqs. (12)–(15) are:

On the heated surface of the rotating solid cylinder :
$$u=-\Omega(Y-Y_0),\ v=\Omega(X-X_0),\ \theta=1. \quad (16)$$
On the left cold wall of the cavity :
$$u=v=0,\ \theta=0,\ X=0,\ Y=1. \quad (17)$$
On the right flexible cold wall of the cavity :
$$u=v=0,\ \theta=0,\ 0\leqslant X\leqslant 1,\ 0\leqslant Y\leqslant 1, \quad (18)$$
$$\frac{\partial\theta}{\partial\mathbf{n}}\quad\text{and}\quad\theta=0. \quad (19)$$
On the horizontal insulated walls : $$\frac{\partial\theta}{\partial X}=\frac{\partial\theta}{\partial Y}=0. \quad (20)$$

The boundary conditions on the flexible right wall are:

$$\frac{\partial\mathbf{d}_s}{\partial\tau}=\mathbf{u}\quad\text{and}\quad E\sigma\cdot\mathbf{n}=-P+Pr\nabla\mathbf{u}. \quad (21)$$

On the taken domain, the absolute velocity was described as [37]:

$$|\mathbf{V}|=|\Omega|R. \quad (22)$$

The revised form of Richardson number which is clearly related to the relative importance of the natural convection and forced convection is written as the following Costa and Raimundo [37]:

$$Ri=\frac{Ra\cdot Pr}{4\Omega^2\cdot R^4} \quad (23)$$

for $\Omega\neq 0$ and the dimensionless cylinder radius $R\neq 0$.

The convective heat transfer at a wall and conduction heat transfer at circular surface are given respectively as

$$q''=h(T_h-T_c),\quad q''=-k\left.\frac{\partial T}{\partial n}\right|_{n=\Theta},$$

where h explains coefficient of the heat transfer, k describes the fluid thermal conductivity and Θ is dimensionless length of the cylinder surface. From the energy balance at a surface, we have

$$h_y(T_h-T_c)=-k\frac{T_h-T_c}{L}\left.\frac{\partial\theta}{\partial n}\right|_{n=\Theta}. \quad (24)$$

The local Nusselt number along the surface of the rotating solid cylinder is written as:

$$Nu=-k\frac{h_yL}{k}=-\left.\frac{\partial\theta}{\partial n}\right|_{n=\Theta}. \quad (25)$$

The average Nusselt number $\overline{Nu}$ is obtained by integrating the local Nusselt number

$$\overline{Nu}=\frac{1}{2\pi}\int_0^{2\pi}Nu\,d\Theta. \quad (26)$$

The average temperature within the whole cavity is computed by the following relation:

$$\theta=\frac{\int\theta_{\text{local}}dA}{\int dA}. \quad (27)$$

The relation of the entropy generation is given by:

$$S=\frac{k_f}{T_0^2}\left[\left(\frac{\partial T}{\partial x}\right)^2+\left(\frac{\partial T}{\partial y}\right)^2\right]+\frac{\mu_f}{T_0}\left[2\left(\frac{\partial u}{\partial x}\right)^2+2\left(\frac{\partial v}{\partial y}\right)^2+\left(\frac{\partial u}{\partial x}+\frac{\partial v}{\partial x}\right)^2\right]. \quad (28)$$

The local entropy generation in the dimensionless form is presented as the following:

$$S_{\text{GEN}}=\left[\left(\frac{\partial\theta}{\partial X}\right)^2+\left(\frac{\partial\theta}{\partial Y}\right)^2\right]+N_\mu\left[4\left(\frac{\partial^2\Psi}{\partial X\partial Y}\right)^2+\left(\frac{\partial^2\Psi}{\partial Y^2}-\frac{\partial^2\Psi}{\partial X^2}\right)^2\right], \quad (29)$$

where $N_\mu=\frac{\mu_fT_0}{k_f}\left(\frac{\alpha_f}{L(\Delta T)}\right)^2$ evaluates the irreversibility distribution ratio and $S_{\text{GEN}}=S_{\text{gen}}\frac{T_0^2L^2}{k_f(\Delta T)^2}$.

Let us denote the first term of Eq. (29) as S_θ, the entropy generation due to the heat transfer irreversibility (HTI) and the second term as S_Ψ, fluid friction irreversibility (NFI). Hence

$$S_{\text{GEN}}=S_\theta+S_\Psi. \quad (30)$$

The global entropy generation (GEG) is achieved by integrating Eq. (30) along the considered domain

$$\text{GEG}=\int S_{\text{GEN}}dXdY=\int S_\theta dXdY+\int S_\Psi dXdY. \quad (31)$$

The Bejan number (Be) is defined as the following:

$$Be=\frac{\int S_\theta dXdY}{\int S_{\text{GEN}}dXdY}, \quad (32)$$

gives the relative strength of the heat transfer irreversibility (HTI) and fluid friction irreversibility (FFI). If $Be>0.5$, then HTI is dominant, while FFI is dominant when $Be<0.5$.

3. Numerical method and validation

The dimensionless governing equations in the arbitrary Lagrangian-Eulerian (ALE) formulation Eqs. (12)–(15) together with dimensionless conditions Eqs. (16)–(21) are solved using the Galerkin Method of Weighted Residuals (Finite Element Method). The governing equation are written in the weak form. Fig. 2 depicts the triangular elements of the discretized computational domain. Then, the discretized equations are written in the form of linear algebraic equations. The damped fully coupled Newton method with the damping factor of 0.9 is utilized [43] to couple the equations of heat, flow, solid structure. A parallel sparse direct solver [44] is employed to solve the algebraic equations. The details of such a procedure are distinctly explained by Reddy [45]. The grid motion is controlled by the Laplace equation to interpret the moving of the structure boundaries. The time steps of the solver are controlled automatically by the implicit free step

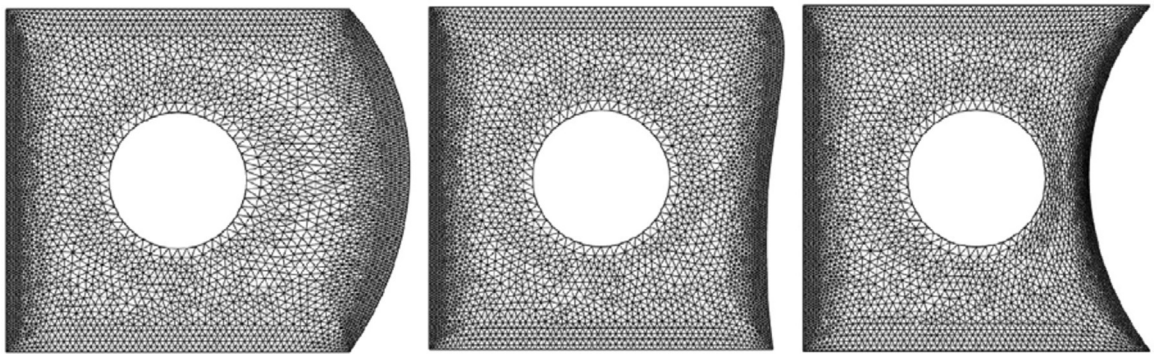

Fig. 2. Grid-points distribution for a grid size 7377 elements (G5).

Backward Differentiation Formula (BDF) with variable order of 1 and 2. The automatic time step ensures the convergence and accuracy of the solution. The convergence criterium used is:

$$\left|\frac{\Gamma^{i+1}-\Gamma^{i}}{\Gamma^{i+1}}\right| \leqslant \eta,$$

where i denotes the iteration number and the convergence criterion η is set at $\eta = 10^{-6}$.

Table 1
Grid testing for $\overline{Nu}, \theta, Be$ and GEG at different grid sizes for $t = 1.5, Ra = 10^6, \Omega = 0.5$ and $E = 10^{13}$.

Grid size	Number of elements	$\overline{Nu}$	θ	Be	GEG
G1	3947	13.614	0.4289	0.011472	5372.6
G2	4463	13.754	0.4179	0.011521	5432
G3	5525	13.85	0.4149	0.011646	5482.6
G4	6287	13.995	0.41191	0.011747	5499.6
G5	7377	14.065	0.41197	0.011749	5555
G6	18409	14.064	0.41196	0.011748	5555.5

We have utilized grids with different sizes to ensure that the present numerical solution is independent on the grid size for the numerical domain, we have used different grid sizes to calculate the average Nusselt number ($\overline{Nu}$), dimensionless temperature (θ), Bejan number (Be) and global entropy generation (GEG) for the steady case ($t = 1.5$), $Ra = 10^6, \Omega = 0.5$ and $E = 10^{13}$. Based on the results examined in Table 1, insignificant differences surrounding the G5 grids and above were observed. Therefore, the G5 non-uniform grid is used to perform all the computations in this paper to solve similar problems as in this subsection.

As a validation, we present in Fig. 3 a comparison between the results of our code with the experimental results described by Nishimura et al. [46] and the numerical findings of Churchill [47] for the problem of natural convection heat transfer inside a square cavity with heated side walls for $Pr = 6.0$. In addition, Fig. 4 shows a comparison with the work of Liao and Lin [48] for the problem of natural convection heat transfer in a square cavity having an embedded heated circular cylinder at $Ra = 2 \times 10^6, R = 0.2$ and $Pr = 7$. In Fig. 5 we compare the average Nusselt number against that of Mehryan et al. [13] for the case of FSI in natural convection heat transfer within a square cavity at $Ra = 10^7, E = 10^{14}, R = 0$ and $Pr = 6.2$. All the comparisons done show very good agreement.

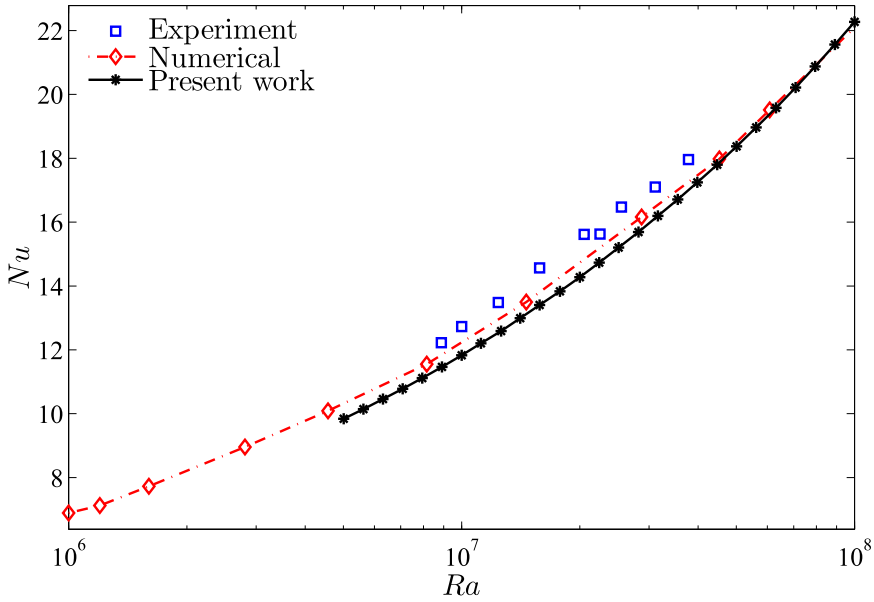

Fig. 3. Comparison between the average Nusselt number of the current numerical work and the experimental data demonstrated by Nishimura et al. [46] and the numerical work based on Churchill's relation by Churchill [47] with Rayleigh number for a rectangular cavity when $AR = 4$ and $Pr = 6$.

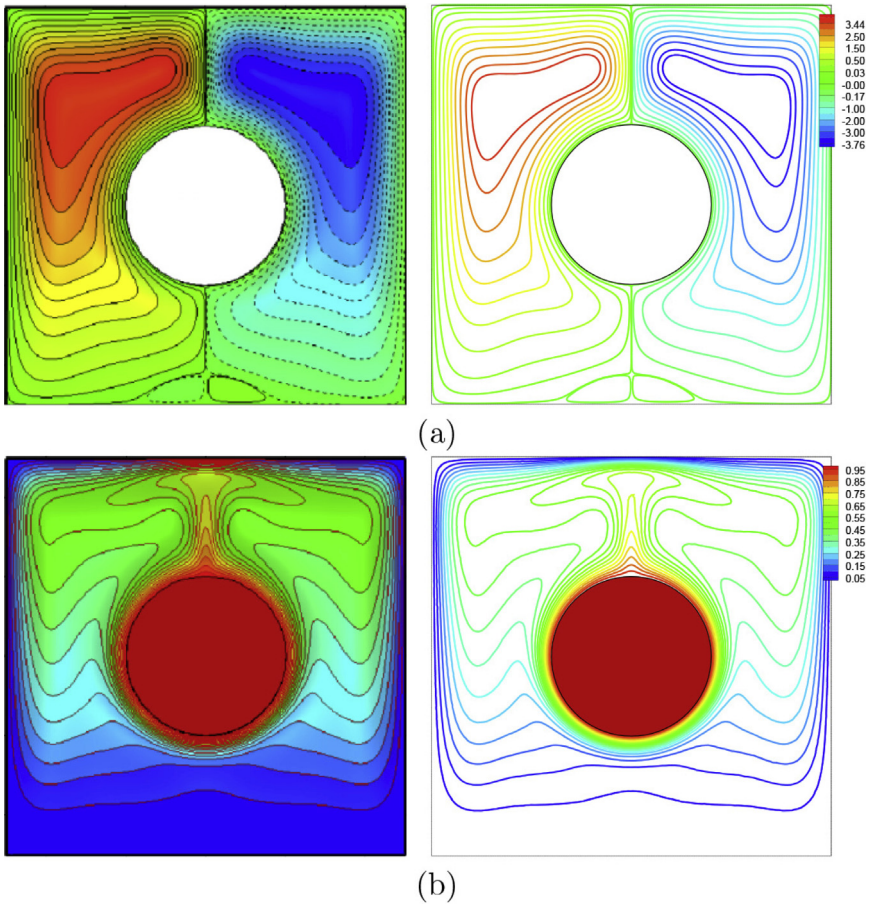

Fig. 4. Streamlines (a), Liao and Lin [48] (left), present study (right), isotherms (b), Liao and Lin [48] (left), present study (right) for $Ra = 2 \times 10^6, R = 0.2$ and $Pr = 7$.

4. Results and discussion

This section presents the numerical outputs for streamlines, isotherms, and isentropic lines (the local dimensionless entropy generation), along with varied dimensionless times $\left(10^{-8} \leqslant \tau \leqslant 3.5\right)$, Rayleigh number $\left(10^4 \leqslant Ra \leqslant 10^7\right)$, angular rotational velocity $(-1 \leqslant \Omega \leqslant 1)$, dimensionless elasticity modulus $(10^{12} \leqslant E \leqslant 10^{15})$, while the values of the thermal conductivity related to the heated circular cylinder, cylinder radius, length of cylinder surface and Prandtl number are fixed at $k_s = 0.76$ W/m·K, $R = 0.2, \Theta = 360$ and $Pr = 4.623$, respectively.

4.1. Role of Rayleigh number

Fig. 6 describes the distribution of streamlines, isotherms and isentropic patterns for various Rayleigh numbers at ($\Omega = 0.5$ and $E = 10^{13}$). Four recirculating zone centers are established adjacent to the rotating cylinder at $Ra = 10^4$ and as Rayleigh number augments, the lower vortex centers disappear and streamlines becomes distorted. Deformation of the right vertical wall is in the negative x direction due to the flexibility of the wall and cylinder rotation. Temperature gradients along the cylinder surface and cold vertical walls become steeper for higher Rayleigh numbers due to the increased effect of natural convection. Local entropy distributions (isotropic) are shown in the last column of Fig. 6 for different values of Rayleigh numbers. At the low Rayleigh number, forced convective effects because the cylinder rotation is effective. Local entropy distributions are higher in the locations for higher temperature gradients along the cylinder surface and vertical walls. For higher values of Rayleigh number, natural convective heat transfer augments and values of local entropy generation becomes higher. Despite the flexibility of the right vertical wall, isentropic distribution near this wall is similar as compared to left vertical rigid wall. Also, for high Rayleigh number ($Ra = 10^7$), local entropy distribution for the right half of the rotating inner cylinder is different as compared to the left part due to the flexibility of the right vertical wall. Since the deformation is in the negative X direction, the distance between the surface of the hot cylinder and the flexible wall becomes reduces and changes the local entropy distribution rates.

Distribution of the steady local Nusselt number for the hot cylinder surface and for the flexible wall in steady configuration are illustrated in Fig. 7 for various Rayleigh numbers ($\Omega = 0.5, E = 10^{14}$). Local enhancement of Nusselt number with Rayleigh number is obtained both for cylinder surface and flexible wall surface. Considering high values of Rayleigh number, secondary peak in the local Nusselt numbers (for right half surface of the hot cylinder and for flexible wall) disappears due to the disappearance of the lower vortex in the right part of the cavity.

Fig. 8 explains the influence of Rayleigh number on the evolution of the time with the average Nusselt number, non-dimensional temperature and Bejan number ($\Omega = 0.5, E = 10^{14}$). After the initial transients die out, the average Nusselt number reaches a constant value and it is higher for higher Rayleigh numbers. Bejan number which represents the ratio of entropy generation rates due to heat transfer and fluid friction shows oscillatory

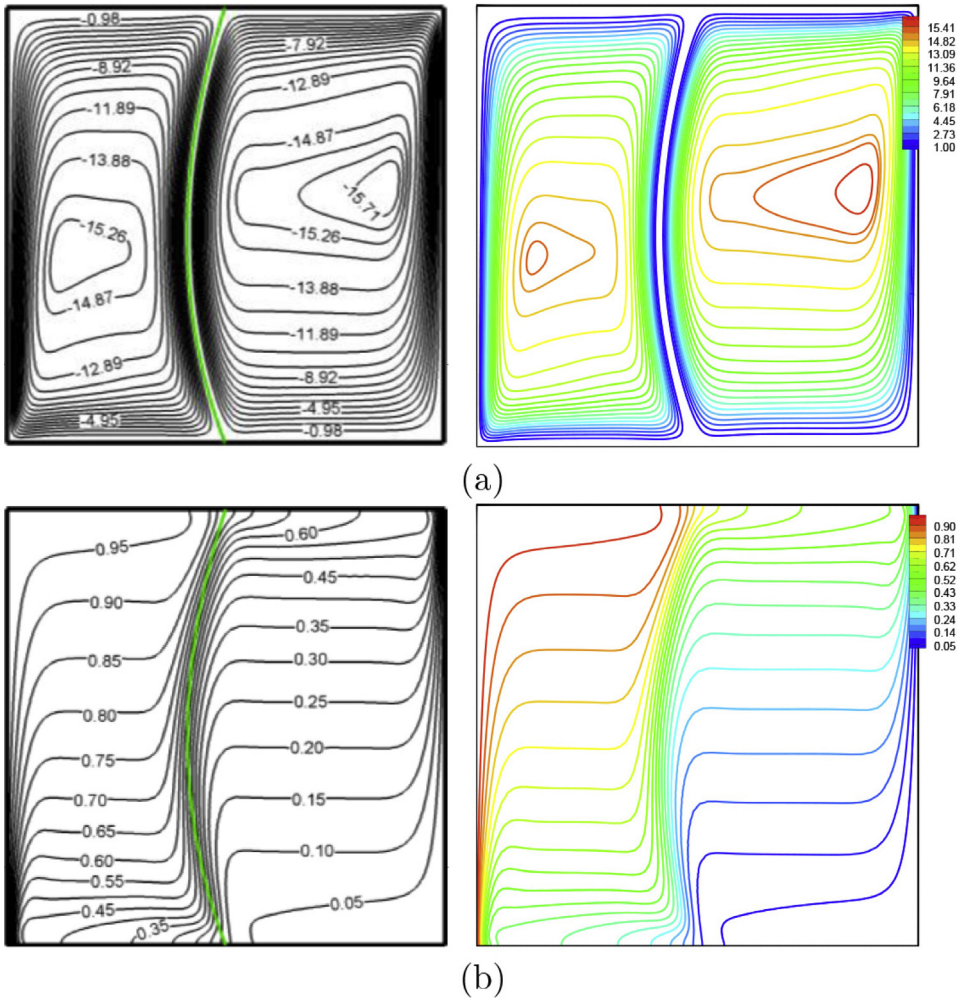

Fig. 5. Streamlines (a), Mehryan et al. [13] (left), present study (right), isotherms (b), Mehryan et al. [13] (left), present study (right) for $Ra = 10^7, E = 10^{14}, R = 0$ and $Pr = 6.2$.

behavior in the initial periods and then reaches higher values for $Ra = 10^4$ and $Ra = 10^5$. A higher value of Rayleigh number results in lower values of Bejan number. For lower values of Rayleigh number, forced convection effects due to inner cylinder rotation is effective and natural convection effects becomes effective for higher values of Rayleigh number. The values of Bejan numbers are below 0.5 which indicates that the entropy generation of the fluid friction irreversibility is dominant over the heat transfer irreversibility.

4.2. Role of angular rotation speed of the inner cylinder

Fig. 9 demonstrates the influence of angular rotation speed related to the hot cylinder on the distribution of streamlines, isotherms and isentropic for fixed values of $Ra = 10^6$ and $E = 10^{13}$. Negative value of Ω indicates the clockwise rotation of the inner cylinder. For stationary cylinder configuration ($\Omega = 0$), flow patterns, thermal patterns and local entropy distributions show a symmetric behavior affected by the vertical axis that passing through the circular cylinder center. Two recirculation zones are established in the left and right parts of the hot cylinder for $\Omega = 0$. A clockwise (counter-clockwise) rotation of the hot cylinder due to the movement of the right flexible wall in the positive (negative) X direction. The path for the hot rising fluid on the circular cylinder surface to the cold cavity wall increases with negative values of Ω for the right part of the cavity and the center vortex in this section moves toward the flexible wall. For the counter-clockwise rotation of the hot cylinder, the flexible wall moves in the negative X direction and the main vortex in the right part of the cavity breaks into two cells. Both for positive and negative value of Ω symmetric flow behavior around the vertical mid axis is not anymore preserved. Isotherm distributions around the circular cylinder and local entropy distributions within the cavity are similar for stationary and clockwise rotation configurations. Considering the counter-clockwise rotation of the hot cylinder at $\Omega = 1$, over the flexible wall and for the right part of the circular cylinder, isotherm distributions become different due to the reduced the gap between the right flexible wall and the surface of the hot cylinder surface and hence the local entropy distributions in those locations vary.

The influence of the hot cylinder angular rotation speed on the local variations of Nusselt number along the hot cylinder surface and flexible wall is demonstrated in Fig. 10 when the steady configuration is considered. Along the hot cylinder surface, local Nusselt number distribution does not change for the clockwise rotation of the hot cylinder (negative value of Ω). When the rotation of the hot cylinder in counter-clockwise direction $\Omega = 1$, an additional peak in the local Nusselt number is established for the hot cylinder surface and for the flexible wall due to the occurrence of the vortex in the lower part of the right flexible wall of the cavity.

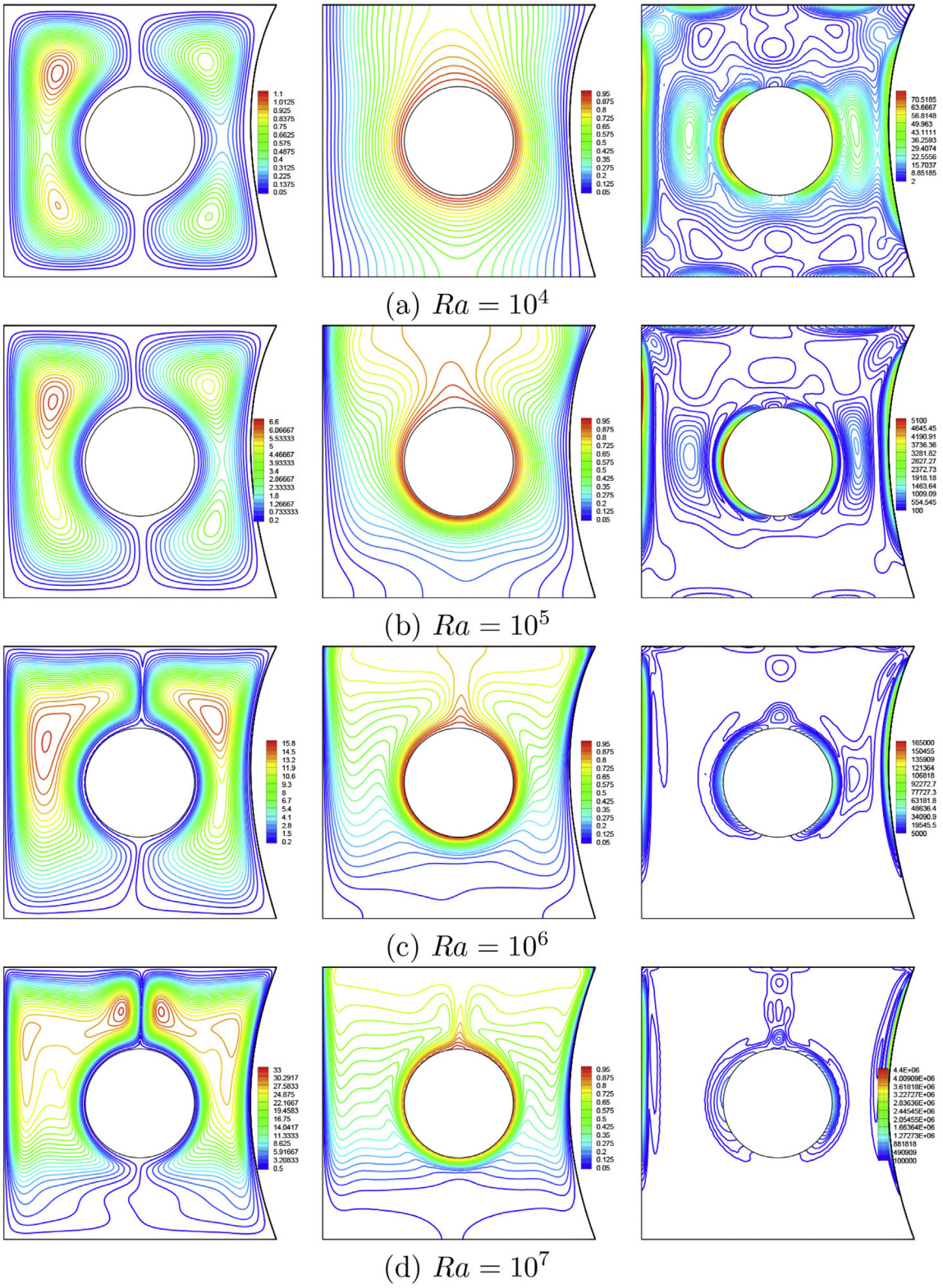

Fig. 6. Variation of the streamlines (left), isotherms (middle), and isentropic (right) evolution by Rayleigh number (Ra) for $\Omega = 0.5$ and $E = 10^{13}$.

The natural convection flow is upward next to the cylinder and down-ward next to the cold walls. When the cylinder rotates in a clockwise direction, it pushes the flow toward the flexible wall with a high momentum reaches the flexible wall. The interaction between the fluid and the flexible wall produces a force toward the right. So, the flexible wall bends outward. The higher the rotation speed, the larger the flexible wall bending. In the case of clockwise rotation, the bending of the wall in outward direction increases the distance between the hot cylinder and the cold wall. Hence, the flow can easily move around the cylinder. However, due

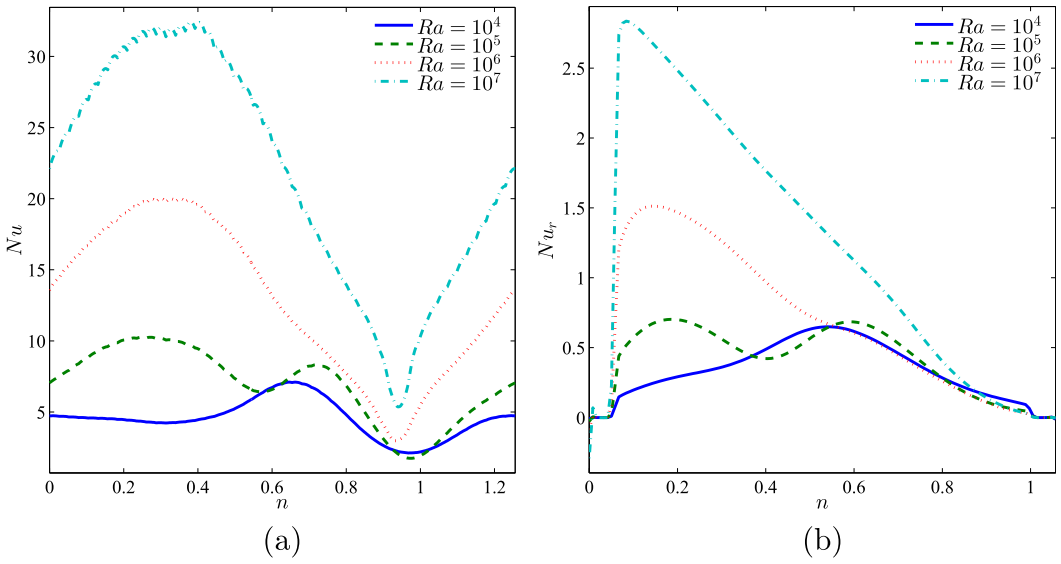

Fig. 7. Variations of the steady local Nusselt number interface with (a) solid cylinder and (b) right flexible wall; for different *Ra* at $\Omega = 0.5$ and $E = 10^{14}$.

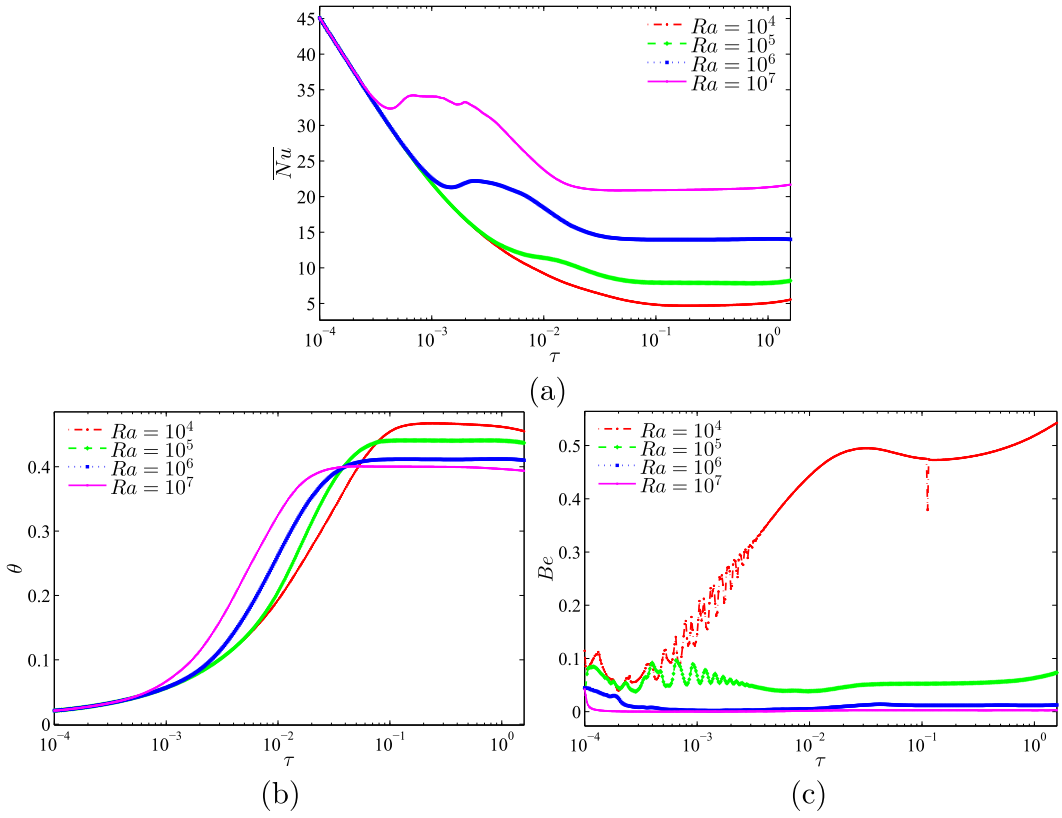

Fig. 8. Variations of the unsteady (a) average Nusselt number, (b) dimensionless temperature and (c) Bejan number with τ for different *Ra* at $\Omega = 0.5$ and $E = 10^{14}$.

to the increase of distance between the wall and cylinder, the velocity and temperature gradient drop. Thus, as seen in the local Nusselt graphs, the rotation of cylinder in the clockwise direction induces a minimal effect on the heat transfer.

In contrast, when the cylinder rotates in the counter-clockwise direction, it pulls the fluid from the flexible wall and pushes the fluid toward the rigid wall. Pulling the fluid from the right side of the cavity reduces the pressure. Due to the reduction of the pressure in the right side of the cavity, the flexible wall bends in an inward direction. Due to the bending of the wall in the inward direction, the distance between the wall and the cylinder as well as the flow passage between the cylinder and the wall reduces. As a result, the rotation flow which easily passes from the left side of the cavity will be passed from a narrow region in the right side of the cavity. In this case, the fluid velocity and the temperature gradients increase significantly. Hence, as seen a distinguished behavior on the local Nusselt number can be observed for the case of counter-clockwise flow.

The angular rotation speed of the hot cylinder shows a negligible influence on the time evolution of the average Nusselt number

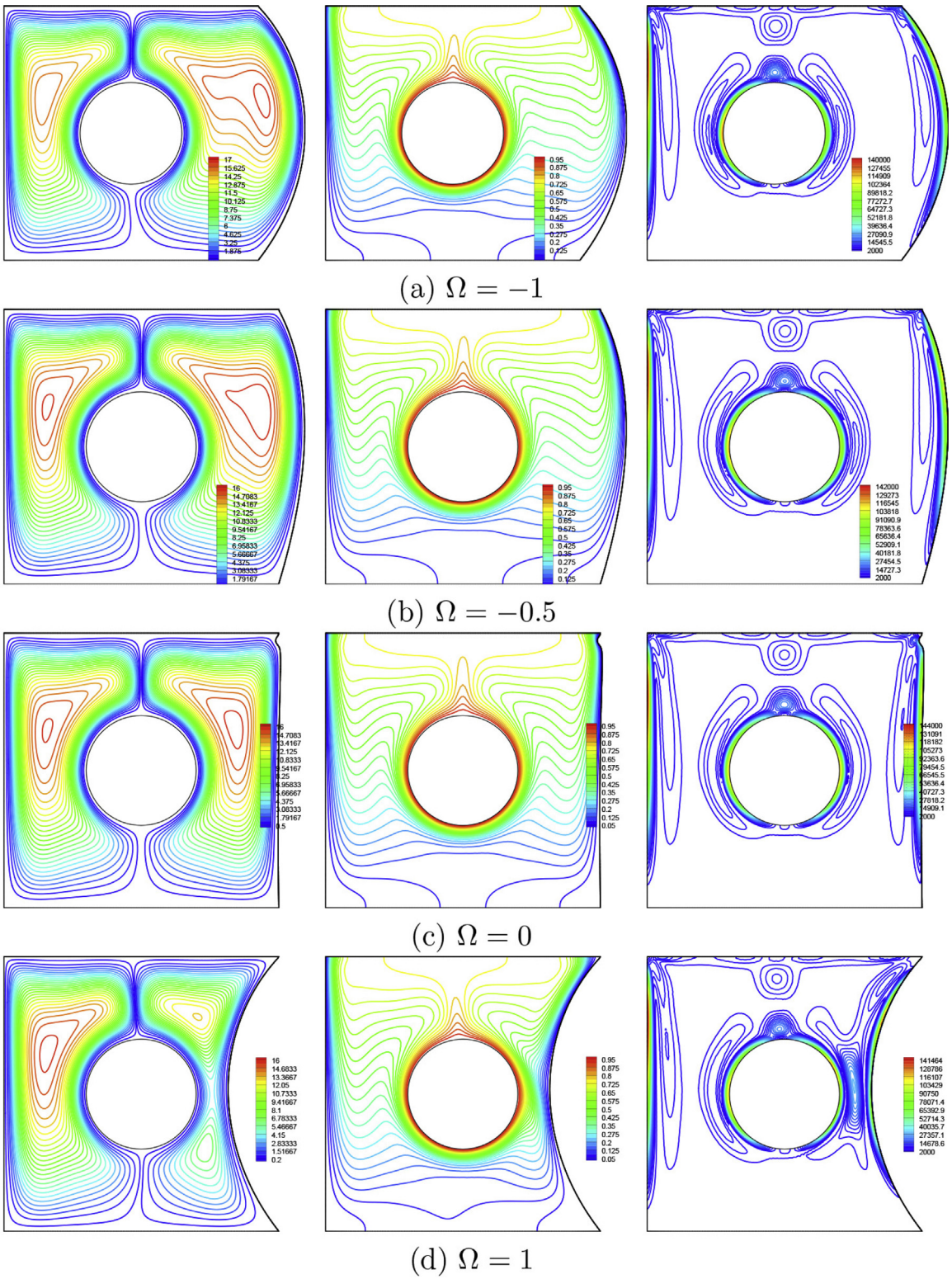

Fig. 9. Variations of the streamlines (left), isotherms (middle), and isentropic (right) evolution by rotational speed (Ω) for $Ra = 10^6$ and $E = 10^{13}$.

for the surface of the inner cylinder (Fig. 11). Even though a local peak was observed in the distribution of the local Nusselt number for the steady configuration, the average value remains constant for the hot cylinder. Bejan number which achieves very low values shows some discrepancies for different Ω values.

Fig. 12 shows the rate of the heat transfer and the dimensionless temperature with Rayleigh number for various angular rotational speed of the hot cylinder. The rotation of the hot cylinder in the clockwise rotation brings weak enhancement (even reduction of the average heat transfer for high Rayleigh numbers is seen) as compared to a motionless cylinder case. The counter-clockwise rotation of the inner hot cylinder results in the enhancement of the heat transfer for the case of lower and higher Rayleigh numbers which could be attributed to the flexible wall deformation in the

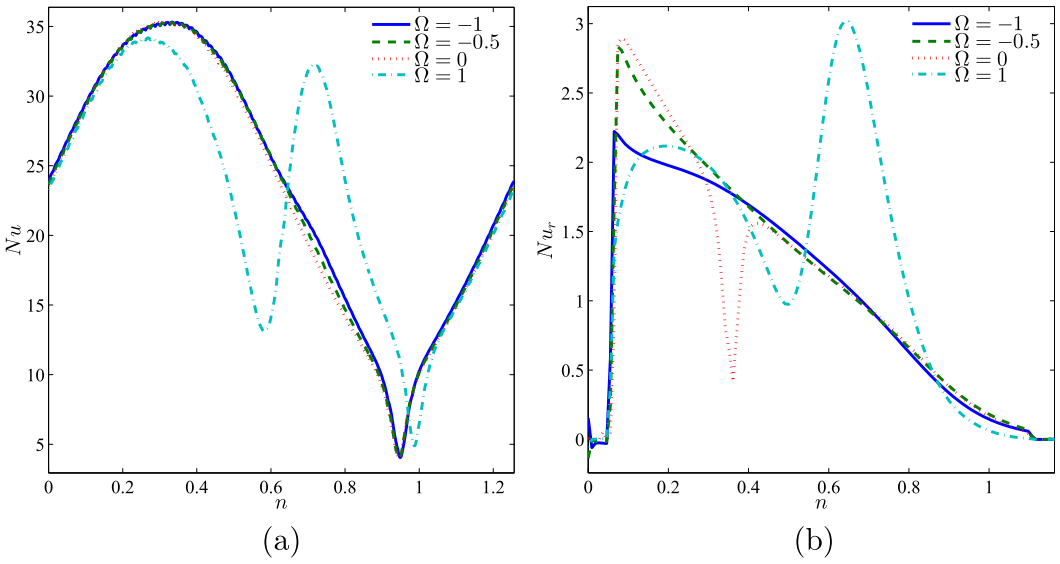

Fig. 10. Variations of the steady local Nusselt number interface with (a) solid cylinder and (b) right flexible wall; for different Ω at $Ra = 10^7$ and $E = 10^{14}$.

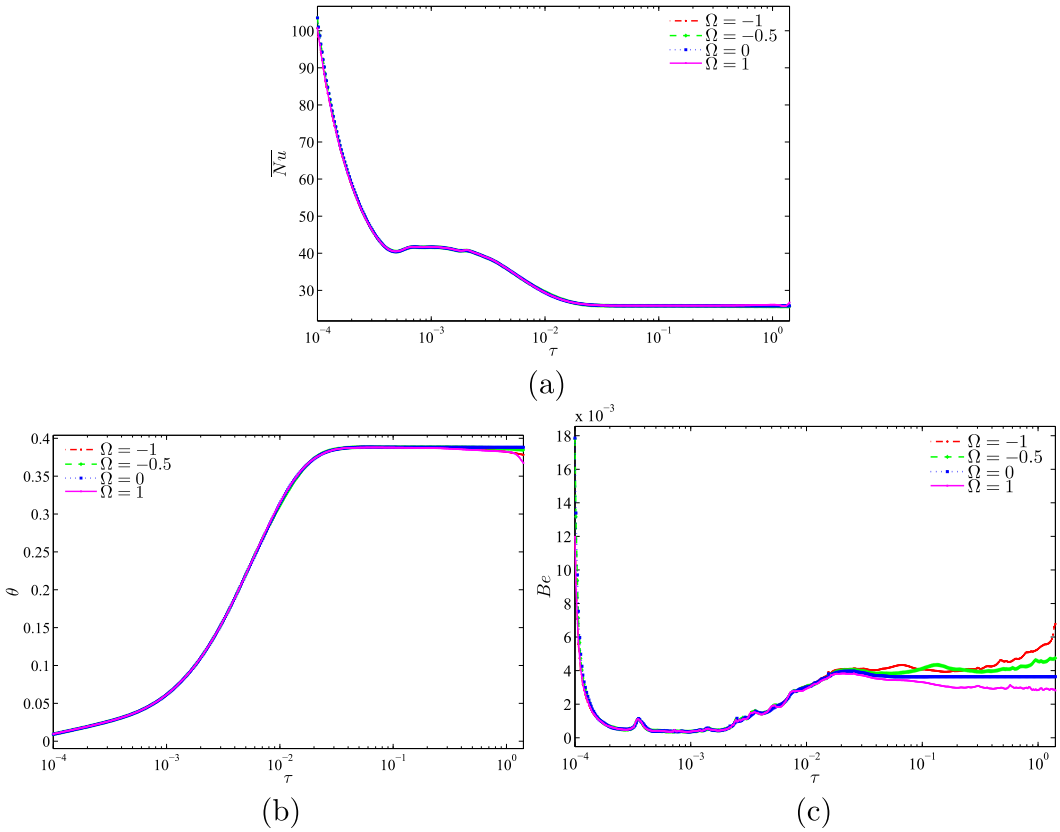

Fig. 11. Variations of the unsteady (a) average Nusselt number, (b) dimensionless temperature and (c) Bejan number with τ for different Ω at $Ra = 10^6$ and $E = 10^{14}$.

negative X direction and vortex break up in the right part of the considered cavity for these flow conditions.

Variations of Bejan number and global entropy generation versus Rayleigh number for different values of Ω are illustrated in Fig. 13 at $E = 10^{14}$. For the higher Rayleigh numbers, irrespective of angular rotation speed of the hot cylinder Bejan number reaches a lower value below than 0.1 which indicates the dominance of fluid friction irreversibility over heat transfer irreversibility which is due to the weak contribution of the rotating cylinder on the total heat transfer rate since the forced convection effect is reduced. At lower values of Rayleigh number, Bejan number is higher for the clockwise rotation of the cylinder (Ω = 1) which denotes that the

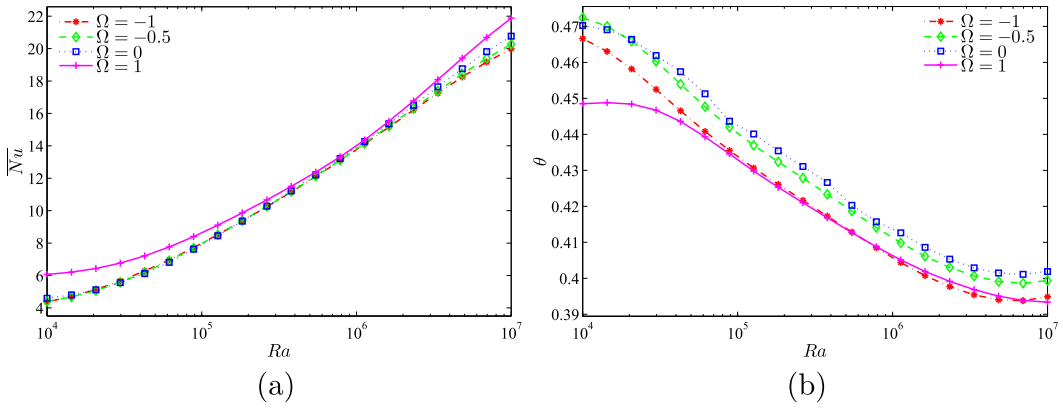

Fig. 12. Variations of the steady (a) average Nusselt number and (b) dimensionless temperature with Ra for different Ω at $E = 10^{14}$.

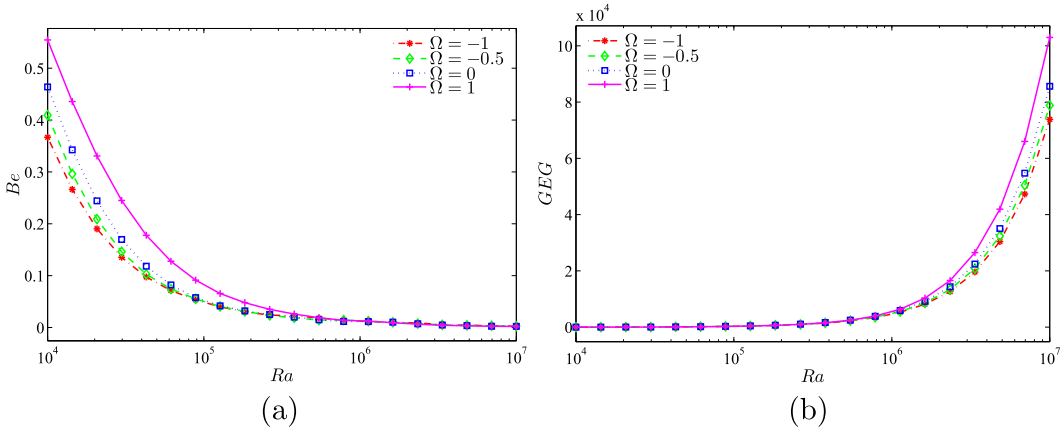

Fig. 13. Variations of the steady (a) Bejan number and (b) global entropy generation (GEG) with Ra for different Ω at $E = 10^{14}$.

irreversibility of the heat transfer is higher as compared to other configurations (for the stationary cylinder or the cylinder that rotates in clockwise direction). This is attributed to the deformation of the flexible wall and formation of the neck with $\Omega = 1$ for counter-clockwise rotation of the inner hot cylinder. The global entropy generation becomes higher with Rayleigh number and achieves the highest value at $Ra = 10^7$ and $\Omega = 1$.

4.3. *Effects of elastic modulus of the flexible right wall*

Variations of flow patterns, thermal patterns and local entropy distributions for various elastic modulus of the flexible right wall are described in Fig. 14 for the counter-clockwise rotation of the hot cylinder ($Ra = 10^7, \Omega = 0.5$). Relying on the non-dimensional elastic modulus of the flexible right wall, different complex shaped wall deformations are observed. For this rotation of the cylinder and for lower elastic modulus values, the upper (lower) part of the elastic wall moves in positive (negative) X direction and a neck which is the locally reduced gap between the inner hot cylinder surface and cold flexible wall is established. The flow patterns in the right half of the cavity are influenced slightly by the variation of wall deformation in different direction for the lower and upper parts of such a region. Along the cold flexible wall, steepening of the thermal gradients and their extensions toward the bottom wall changes due to the wall deformation. Along the hot circular cylinder, isotherm distributions look similar for different elastic modulus values since the neck is not small enough which depends on the value and the direction of the rotational speed of the inner hot cylinder. Local entropy distribution changes especially adjacent to the flexible wall and hot cylinder surface for a variety elastic modulus values.

The average Nusselt number, Bejan number and global entropy generation versus non-dimensional angular rotation speed of the hot cylinder for various elastic modulus of the right flexible wall are demonstrated in Fig. 15 and Fig. 16 when the Rayleigh number is fixed to value of 10^6. The counter-clockwise rotation of the inner hot cylinder leads to a strong enhancement on the rate of the heat transfer, such a behaviour was achieved by applying lower elastic modulus when the right wall is more flexible. Even though the global entropy generation enhances with positive values of Ω and for lower elastic modulus, Bejan number reaches very low values in the parametric range of interest. In this case, the fluid friction irreversibility is dominant over heat transfer irreversibility.

When the elastic modulus is low, the flexible wall would easily deform due to the pressure gradients and interaction with the fluid. In the case of $E = 10^{12}$, the wall is very flexible; hence, the wall is under the significant influence of fluid interaction. The natural convection flow is in an upward direction next to the cylinder and a downward direction next to the flexible wall. The counter-clockwise rotation of the cylinder aids the natural convection fluid around the cylinder to move upward and prevents the cold fluid next to the flexible wall to fall. Hence, the upper part of the wall

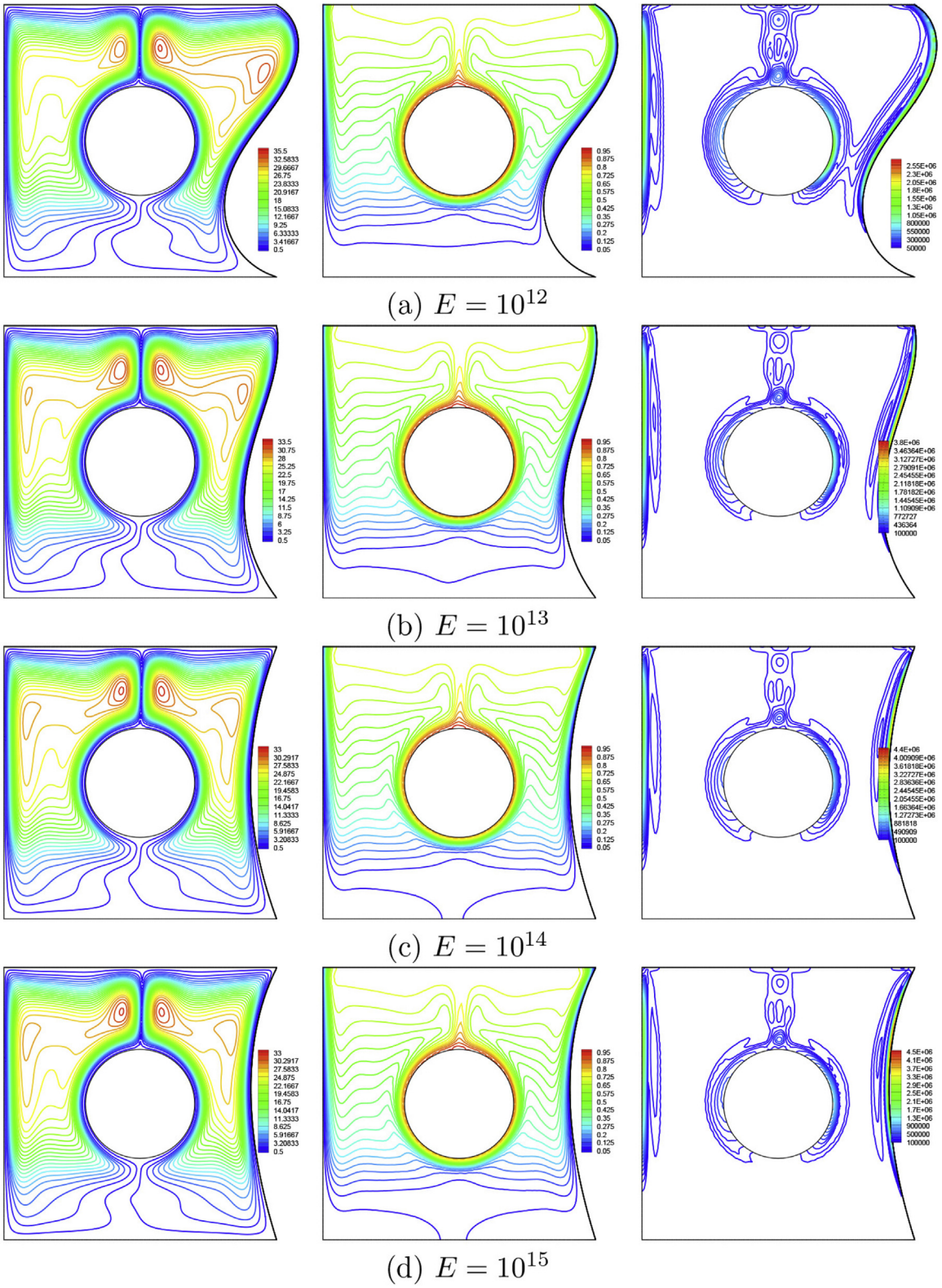

Fig. 14. Variation of the streamlines (left), isotherms (middle), and isentropic (right) evolution by dimensionless elasticity modulus (E) for $Ra = 10^7$ and $\Omega = 0.5$.

bent in the outward direction. In the bottom of the cavity, there is a low-pressure region which pulls the flexible wall inward. When the elastic modulus increases, the flexibility of the wall decreases, and it only reacts to the dominant forces, originated from the rotation of the cylinder. Consequently, the dimensionless temperature and average Nusselt number follow the behavior of the flexible wall. When the elastic modulus of the flexible wall is low, the patterns of the dimensionless temperature and average Nusselt number shift from asymmetric behavior toward a non-symmetric behavior.

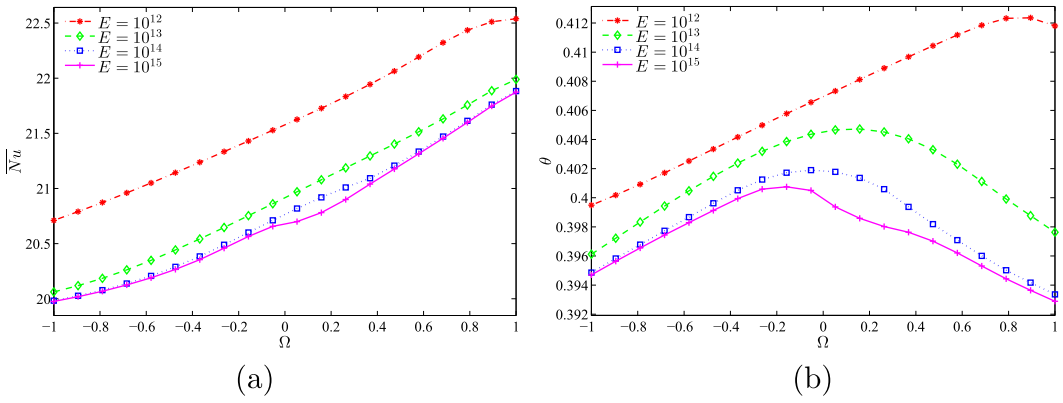

Fig. 15. Variations of the steady (a) average Nusselt number and (b) dimensionless temperature with Ω for different E at $Ra = 10^6$.

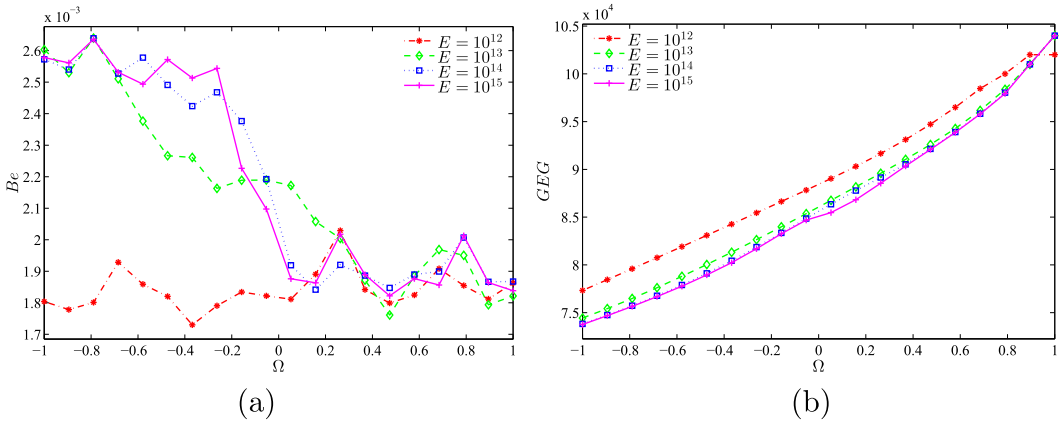

Fig. 16. Variations of the steady (a) Bejan number and (b) global entropy generation (GEG) with Ω for different E at $Ra = 10^6$.

5. Conclusions

In the current investigation, numerical analysis of entropy generation and mixed convective heat transfer due to an inner hot rotating cylinder inside a cavity with flexible right wall were performed. We have concluded the following important results:

- Local and average Nusselt numbers augment with Rayleigh number increment and secondary peak in the local Nusselt number is established (for right half surface of the hot cylinder and for flexible wall) for lower values of Rayleigh number due to the formation of the lower vortex in the right behalf of the considered cavity.
- A higher value of Rayleigh number results in lower values of Bejan number which are are below 0.5 which indicates the entropy generation due to the domination of the fluid friction irreversibility.
- Clockwise or counter-clockwise rotation of the hot inner cylinder results in various deformation paths of the flexible wall which has different effects on the entropy generation and convection heat transfer.
- For the counter-clockwise directional rotation of the hot cylinder, secondary peak in the local Nusselt number is obtained for the hot cylinder surface and for the flexible wall due to the formation of the vortex. However, local Nusselt number does not change for clockwise rotation of the hot cylinder even though the wall deformation is in positive X direction.
- Different complex shaped wall deformations are established depending on the non-dimensional elastic modulus of the flexible right wall.
- The highest values of average Nusselt number are obtained for the counter-clockwise rotation of the hot cylinder and when the flexible wall is moving with lower elastic modulus.
- The global entropy generation rate rises with counter-clockwise rotation of the hot cylinder and for lower values of elastic modulus but the Bejan number achieves very low values in the parametric range of interest.

The results of the present study show that using a very flexible wall can significantly affect the flow and heat transfer in the cavity. The change in the flow behavior would change the shape of the flexible wall which in return it would affect the flow and heat transfer. Hence, using a flexible wall can be a new way for passive control of flow and heat transfer in engineering application.

Acknowledgments

We are grateful for the financial support received from Malaysia's Ministry of Higher Education under the grant GSP/1/2015/SG04/UKM/01/1.

References

[1] A.I. Alsabery, M.A. Ismael, A.J. Chamkha, I. Hashim, Mixed convection of Al2O3-water nanofluid in a double lid-driven square cavity with a solid inner insert using Buongiorno's two-phase model, Int. J. Heat Mass Transf. 119 (2018) 939–961.
[2] H.F. Öztop, I. Dagtekin, Mixed convection in two-sided lid-driven differentially heated square cavity, Int. J. Heat Mass Transf. 47 (2004) 1761–1769.
[3] F. Talebi, A.H. Mahmoudi, M. Shahi, Numerical study of mixed convection flows in a square lid-driven cavity utilizing nanofluid, Int. Commun. Heat Mass Transf. 37 (2010) 79–90.

[4] E. Abu-Nada, A.J. Chamkha, Mixed convection flow in a lid-driven inclined square enclosure filled with a nanofluid, Eur. J. Mech. B/Fluids 29 (2010) 472–482.
[5] A. Rashad, S. Abbasbandy, A.J. Chamkha, Mixed convection flow of a micropolar fluid over a continuously moving vertical surface immersed in a thermally and solutally stratified medium with chemical reaction, J. Taiwan Inst. Chem. Eng. 45 (2014) 2163–2169.
[6] G. Ramesh, A. Chamkha, B. Gireesha, Boundary layer flow past an inclined stationary/moving flat plate with convective boundary condition, Afrika Matematika 27 (2016) 87–95.
[7] M. Raju, A. Chamkha, J. Philip, S. Varma, Soret effect due to mixed convection on unsteady magnetohydrodynamic flow past a semi infinite vertical permeable moving plate in presence of thermal radiation, heat absorption and homogenous chemical reaction, Int. J. Appl. Comput. Math. 3 (2017) 947–961.
[8] A.J. Chamkha, A.M. Rashad, M.A. Mansour, T. Armaghani, M. Ghalambaz, Effects of heat sink and source and entropy generation on MHD mixed convection of a Cu-water nanofluid in a lid-driven square porous enclosure with partial slip, Phys. Fluids 29 (2017) 052001.
[9] A.K. Kareem, S. Gao, Computational study of unsteady mixed convection heat transfer of nanofluids in a 3D closed lid-driven cavity, Int. Commun. Heat Mass Transf. 82 (2017) 125–138.
[10] A.I. Alsabery, M.A. Sheremet, A.J. Chamkha, I. Hashim, Impact of nonhomogeneous nanofluid model on transient mixed convection in a double lid-driven wavy cavity involving solid circular cylinder, Int. J. Mech. Sci. 150 (2019) 637–655.
[11] A. Al-Amiri, K. Khanafer, Fluid–structure interaction analysis of mixed convection heat transfer in a lid-driven cavity with a flexible bottom wall, Int. J. Heat Mass Transf. 54 (2011) 3826–3836.
[12] M. Engel, M. Griebel, Flow simulation on moving boundary-fitted grids and application to fluid–structure interaction problems, Int. J. Numer. Meth. Fluids 50 (2006) 437–468.
[13] S. Mehryan, M. Ghalambaz, M.A. Ismael, A.J. Chamkha, Analysis of fluid-solid interaction in mhd natural convection in a square cavity equally partitioned by a vertical flexible membrane, J. Magn. Magn. Mater. 424 (2017) 161–173.
[14] X. Shi, J. Khodadadi, Fluid flow and heat transfer in a lid-driven cavity due to an oscillating thin fin: transient behavior, Trans. ASME-C-J. Heat Transf. 126 (2004) 924–930.
[15] X. Shi, J. Khodadadi, Periodic state of fluid flow and heat transfer in a lid-driven cavity due to an oscillating thin fin, Int. J. Heat Mass Transf. 48 (2005) 5323–5337.
[16] J.P. Gomes, H. Lienhart, Fluid–structure interaction-induced oscillation of flexible structures in laminar and turbulent flows, J. Fluid Mech. 715 (2013) 537–572.
[17] C.-H. Ku, Flexible heat transfer assembly, 2015. US Patent App. 14/084,284.
[18] A.I. Alsabery, M.A. Sheremet, A.J. Chamkha, I. Hashim, MHD convective heat transfer in a discretely heated square cavity with conductive inner block using two-phase nanofluid model, Sci. Rep. 8 (2018) 7410.
[19] A.K. Soti, R. Bhardwaj, J. Sheridan, Flow-induced deformation of a flexible thin structure as manifestation of heat transfer enhancement, Int. J. Heat Mass Transf. 84 (2015) 1070–1081.
[20] M. Ghalambaz, E. Jamesahar, M.A. Ismael, A.J. Chamkha, Fluid-structure interaction study of natural convection heat transfer over a flexible oscillating fin in a square cavity, Int. J. Therm. Sci. 111 (2017) 256–273.
[21] A.A. Dey, Y. Modarres-Sadeghi, J.P. Rothstein, Experimental observation of viscoelastic fluid–structure interactions, J. Fluid Mech. 813 (2017).
[22] F. Selimefendigil, H.F. Öztop, Laminar convective nanofluid flow over a backward-facing step with an elastic bottom wall, J. Therm. Sci. Eng. Appl. 10 (2018) 041003.
[23] F. Selimefendigil, H.F. Öztop, A.J. Chamkha, Analysis of mixed convection and entropy generation of nanofluid filled triangular enclosure with a flexible sidewall under the influence of a rotating cylinder, J. Therm. Anal. Calorim. (2018), https://doi.org/10.1007/s10973-018-7317-5.
[24] A. Raisi, I. Arvin, A numerical study of the effect of fluid-structure interaction on transient natural convection in an air-filled square cavity, Int. J. Therm. Sci. 128 (2018) 1–14.
[25] M.A. Ismael, H.F. Jasim, Role of the fluid-structure interaction in mixed convection in a vented cavity, Int. J. Mech. Sci. 135 (2018) 190–202.
[26] A. Alsabery, M. Ismael, A. Chamkha, I. Hashim, Numerical investigation of mixed convection and entropy generation in a wavy-walled cavity filled with nanofluid and involving a rotating cylinder, Entropy 20 (2018) 664.
[27] M.A. Sheremet, H.F. Oztop, I. Pop, N. Abu-Hamdeh, Analysis of entropy generation in natural convection of nanofluid inside a square cavity having hot solid block: Tiwari and Das' model, Entropy 18 (2015) 9.
[28] N.S. Bondareva, M.A. Sheremet, H.F. Oztop, N. Abu-Hamdeh, Entropy generation due to natural convection of a nanofluid in a partially open triangular cavity, Adv. Powder Technol. 28 (2017) 244–255.
[29] M. Sheremet, I. Pop, H.F. Öztop, N. Abu-Hamdeh, Natural convection of nanofluid inside a wavy cavity with a non-uniform heating: Entropy generation analysis, Int. J. Numer. Methods Heat Fluid Flow 27 (2017) 958–980.
[30] I. Hashim, A.I. Alsabery, M.A. Sheremet, A.J. Chamkha, Numerical investigation of natural convection of Al2O3-water nanofluid in a wavy cavity with conductive inner block using Buongiorno's two-phase model, Adv. Powder Technol. 30 (2019) 399–414.
[31] A.I. Alsabery, T. Tayebi, A.J. Chamkha, I. Hashim, Effect of rotating solid cylinder on entropy generation and convective heat transfer in a wavy porous cavity heated from below, Int. Commun. Heat Mass Transf. 95 (2018) 197–209.
[32] W.-S. Fu, C.-S. Cheng, W.-J. Shieh, Enhancement of natural convection heat transfer of an enclosure by a rotating circular cylinder, Int. J. Heat Mass Transf. 37 (1994) 1885–1897.
[33] N.K. Ghaddar, Natural convection over rotating cylindrical heat source in an enclosure, J. Thermophys. Heat Transf. 10 (1996) 303–311.
[34] T. Kimura, M. Takeuchi, N. Nagai, T. Yoshida, Heat transfer control in an enclosure by using a rotating plate and stratified fluids, Heat Transfer—Asian, Research 32 (2003) 489–500.
[35] H.F. Oztop, Z. Zhao, B. Yu, Fluid flow due to combined convection in lid-driven enclosure having a circular body, Int. J. Heat Fluid Flow 30 (2009) 886–901.
[36] S.B. Paramane, A. Sharma, Numerical investigation of heat and fluid flow across a rotating circular cylinder maintained at constant temperature in 2-D laminar flow regime, Int. J. Heat Mass Transf. 52 (2009) 3205–3216.
[37] V. Costa, A. Raimundo, Steady mixed convection in a differentially heated square enclosure with an active rotating circular cylinder, Int. J. Heat Mass Transf. 53 (2010) 1208–1219.
[38] S.H. Hussain, A.K. Hussein, Mixed convection heat transfer in a differentially heated square enclosure with a conductive rotating circular cylinder at different vertical locations, Int. Commun. Heat Mass Transf. 38 (2011) 263–274.
[39] C.-C. Liao, C.-A. Lin, Mixed convection of a heated rotating cylinder in a square enclosure, Int. J. Heat Mass Transf. 72 (2014) 9–22.
[40] D. Chatterjee, S.K. Gupta, B. Mondal, Mixed convective transport in a lid-driven cavity containing a nanofluid and a rotating circular cylinder at the center, Int. Commun. Heat Mass Transf. 56 (2014) 71–78.
[41] K. Khanafer, S.M. Aithal, Mixed convection heat transfer in a lid-driven cavity with a rotating circular cylinder, Int. Commun. Heat Mass Transf. 86 (2017) 131–142.
[42] A.I. Alsabery, M.A. Sheremet, M. Ghalambaz, A.J. Chamkha, I. Hashim, Fluid-structure interaction in natural convection heat transfer in an oblique cavity with a flexible oscillating fin and partial heating, Appl. Therm. Eng. 145 (2018) 80–97.
[43] P. Wriggers, Nonlinear Finite Element Methods, Springer Science & Business Media, 2008.
[44] P.R. Amestoy, I.S. Duff, J.-Y. L'excellent, Multifrontal parallel distributed symmetric and unsymmetric solvers, Comput. Methods Appl. Mech. Eng. 184 (2000) 501–520.
[45] J.N. Reddy, An Introduction to the Finite Element Method, vol. 2, McGraw-Hill, New York, 1993.
[46] T. Nishimura, M. Shiraishi, F. Nagasawa, Y. Kawamura, Natural convection heat transfer in enclosures with multiple vertical partitions, Int. J. Heat Mass Transf. 31 (1988) 1679–1686.
[47] S.W. Churchill, Free convection in layers and enclosures, in: G.F. Hewitt, exec. (ed.), Heat Exchanger Design Handbook, Section 2.5.8, Begell House, New York, 2002.
[48] C.-C. Liao, C.-A. Lin, Influence of Prandtl number on the instability of natural convection flows within a square enclosure containing an embedded heated cylinder at moderate rayleigh number, Phys. Fluids 27 (2015) 013603.